Influence of the pointing direction and detector sensitivity variations on the detection rate of a double station meteor camera

Thomas Albin[1, 2], Detlef Koschny[3,4], Gerhard Drolshagen[3], Rachel Soja[1], Ralf Srama[1] and Bjoern Poppe[2]

[1] **Institute of Space Systems, University of Stuttgart, Pfaffenwaldring 29, 70569 Stuttgart, Germany**
albin@irs.uni-stuttgart.de, soja@irs.uni-stuttgart.de, srama@irs.uni-stuttgart.de

[2] **Universitätssternwarte Oldenburg, Institute of Physics and Department of Medical Physics and Acoustics, Carl von Ossietzky University, 26129 Oldenburg, Germany**
bjoern.poppe@uni-oldenburg.de

[3] **European Space Agency, ESA/ESTEC, Keplerlaan 1, 2201 AZ Noordwijk ZH, Netherlands**
detlef.koschny@esa.int, gerhard.drolshagen@esa.int

[4] **Chair of Astronautics, Technical Univ. Munich, Boltzmannstraße 15, 85748 Garching, Germany**

The Canary Islands Long-Baseline Observatory (CILBO) is a double station meteor observation site on Tenerife and La Palma (Koschny et al., 2013; Koschny et al., 2014). Meteors are detected within the 40 ms long video frames of the identically built cameras using MetRec (Molau, 1999). MOTS (version 3, Koschny & Diaz, 2002) is used to determine the meteor trajectories of double-station observations. First scientific results regarding the velocity distribution and meteoroid flux have been published by Drolshagen et al., 2014 and Ott et al., 2014. Both authors found effects related to the Apex direction, such as an increasing number of detections in the morning hours. Sporadic meteors from the Apex cause additional observational bias, including in the velocity-magnitude domain and the meteor trail length determination. We show how the detection threshold conditions vary depending on the pointing direction of the cameras for both CILBO cameras. The angular velocity distribution of the meteors depends on the camera orientation. Meteors with a smaller angular velocity illuminate less CCD pixels in the same time interval than faster meteors causing a higher Signal-to-Noise ratio and consequently better detection threshold conditions. Additionally, we analyzed the detection distribution within the field of view of the CILBO cameras. We quantified this effect, which can be attributed mainly to vignetting in the wide-angle system.

1 Introduction

CILBO (Canary Islands Long-Baseline Observatory) is a double station meteor camera system consisting of cameras on the Canary Islands of Tenerife and La Palma, named ICC7 and ICC9 respectively (Koschny et al., 2013). Both systems are image intensified video cameras. An additional camera is installed on Tenerife with an optical grid for spectral analysis of meteors – named ICC8. CILBO has been installed in July 2011 and operates continuously since January 2013. The 40 ms long video frames are analyzed in real-time with MetRec (Molau, 1999). Meteors, which appear on more than two video frames are considered for further analysis.

Both cameras have a similar setup and their optical axis are aligned to the same geographical coordinate. The overlapping Field-of-Views (FOVs) of both cameras (28 x 22 deg^2), their position and detection volume can be seen in *Figure 1*. The alignment of ICC7 and ICC9 allows a stereoscopic observation of meteors which move across the FOV of both cameras. Meteors which have been simultaneously detected by MetRec are analyzed and a trajectory along the overlapping detection volume is computed (see *Figure 1*). Each dot represents the photometric center of the meteor on each individual video frame. These data are then used by the program MOTS to reconstruct the orbit and determine the Keplerian elements of each meteor (Koschny and Diaz, 2002). Currently (31.05.2015) 11785 meteors have been observed simultaneously. A brief overview of the CILBO system and its functionality are given in Koschny et al. (2014). The current status of the Meteor Research Group are provided in Koschny et al. (2015).

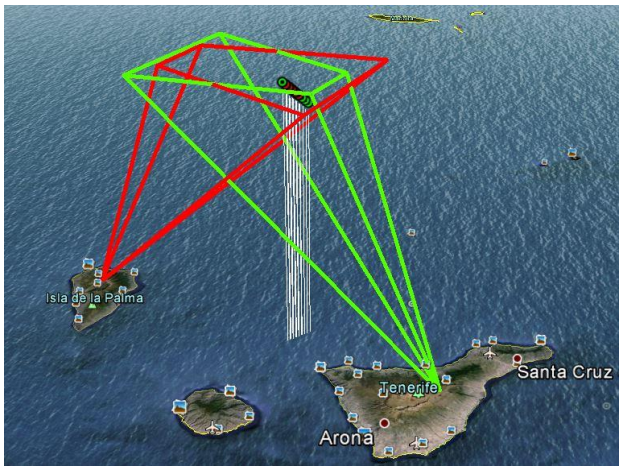

Figure 1 – Field of View of both CILBO cameras (La Palma: ICC9, Tenerife: ICC7). The dots show the position determination of a meteor observed by ICC9 and ICC7, respectively. The meteor is within the overlapping FOV volume. FOV data from Koschny (personal communication, 2015).

First scientific results have been obtained by Drolshagen

et al. (2014) and Ott et al. (2014). Both used 6663 meteor data of simultaneous detections during the time period June 2013 until May 2014. Ott et al. (2014) used the CILBO data to determine the mass distribution of the meteors and the mass influx on Earth. They found partial agreement between the CILBO derived data and the Grün model (Grün et al., 1985). Some system inherent bias has been described which is the subject of additional investigations presented in this proceedings (Drolshagen et al., 2015, Kretschmer et al., 2015). Drolshagen et al. (2014) determined the velocity distribution of the meteors and compared their results with the Space Environment Standard of the European Cooperation for Space Standardization (ECSS 2008). The ECSS model is based on radio observations by the Harvard Radio Meteor Project in the late 1960's. Drolshagen et al. (2014) found additionally an Apex effect in the velocity data set. The distribution showed a significant peak at high velocities (around and above 60 km/s) which is an effect of the Earth's motion around the Sun.

This paper is a technical analysis of the CILBO system considering further Apex and camera pointing depending effects. First of all the data format of the CILBO system is explained. Afterwards we will show and explain in Section 3 the Apex effects and the resulting bias in our data sets. Understanding these effects is a crucial point to de-bias especially the meteor brightness and velocity data for further studies. Afterwards Section 4 describes the sensitivity of the CILBO camera. Here, meteor data have been used for calibration and de-biasing purposes.

The analysis in this paper uses new Machine Learning based approaches like e.g. Gaussian Processes, Kernel Density Estimators or Gaussian Mixture Models. The used software libraries are "SciKit" (Pedregosa et al., 2011) and "AstroML" (Vanderplas et al., 2012). A detailed description of the algorithms, the mathematical background and additional information for applications in astrophysics can be found in Vanderplas et al. (2014). We used these approaches like, including Kernel Density Estimators as an alternative to classical histograms, which can lead to severely statistical bias if using not correctly.

2 CILBO's file format

Both CILBO cameras work autonomously. Meteors are detected by MetRec (Molau, 1999) and saved if the number of video frames is 3 or larger. A video frame is 40 ms long. For each frame the magnitude of the meteor is determined as well as the photometric center in CCD- and equatorial coordinates. The CCD coordinates are an arbitrarily defined coordinate system ranging from 0 to 1 along the width (768 pixels) and height (576 pixels) of the CCD chip. Equatorial coordinates of the meteor position are computed with a reference star catalog. These data are saved in so called inf-files.

These inf-files are used by a program to determine simultaneously detected meteors by ICC7 and ICC9. A trajectory of a stereoscopically observed meteor is computed and saved in a so called "Detailed Altitude File" (daf). The software MOTS (Koschny and Diaz, 2002) use these files to compute the orbital elements of the meteors in helio-centric coordinates outside of the gravitational vicinity of Earth. An exemplary daf-file can be seen in Drolshagen et al. (2014).

Figure 6 shows a meteor trail detected by ICC7 and ICC9 on 2015-05-08.

3 Pointing-dependent bias

As previously shown in *Figure 1*, ICC7 and ICC9 are located on Tenerife and La Palma, respectively. Their geographical coordinates have been obtained from Koschny et al. (2014) and are shown in the first 2 rows of *Table 1*. The third row lists the geographical coordinate and elevation of the so called aim point. Both optical axis vectors of ICC7 and ICC9 (in the following called boresight) are aligned to this point which is allocated between both islands.

Table 1 – Geographical latitude (North) and longitude (West) of both CILBO cameras and the aim point. Both cameras boresights intersect at an altitude of 100 km. From Koschny et al. (2014).

Island	Camera	Lat. (N)	Long. (W)	Elevation
Tenerife	ICC7/8	28°18'04"	16°30'43"	2395 m
La Palma	ICC9	28°45'36"	17°52'57"	2327 m
Aim Point		28°32'00"	17°10'00"	100 km

The analysis of this Section determines whether camera pointing dependent bias is present in the current data set of simultaneously detected meteors. A first approach is given by Drolshagen et al. (2014). They determined a meteor flight direction bias and an increase of meteor detections during the morning hours due to the Apex contribution. Here we analyze the effects in more detail. For our analysis we use the entire CILBO meteor dataset including sporadic meteors as well as stream meteors.

For the analysis we use the daf-files which contain all simultaneously observed meteor data. Each daf-file contains n_1 and n_2 video frames of a meteor as seen from ICC7 and ICC9, respectively. The minimum number of video frames is 3 per camera. For each daf-file the program MOTS computes n_1 - 1 and n_2 - 1 velocities by comparing the meteor position and distance to the camera between two frames. These values and the corresponding brightness measurements are used for *Figures 2 and 3*. Both Figures show the 2-dimensional probability density function (PDF) in the velocity - magnitude domain from 0 km/s to 80 km/s and from -2.5 mag to +8 mag. The data points are fitted using a Gaussian Mixture Model (GMM). The GMM fits the data with a different number of 2-dimensional Gaussian distributions. For each model the Bayesian Information Criterion (BIC) value is computed. This value contains the maximum likelihood function and a penalty term depending on the number of chosen mode parameters. This information criterion can

be described as a mathematical description of "Occam's Razor". The model with the smallest BIC value is the preferred solution. In both cases the best model is a mixture of 4 underlying Gaussians. Two Gaussians describe two major data point clusters that correspond here to the two local probability densities maxima. Two additional Gaussians describe the data background. To verify the clusters an additional clustering algorithm (K-Means) is applied, too. This algorithm searches for local density maxima by comparing the number of nearby data points within a certain threshold. The computed cluster centers are represented by the white dots and fit with the maxima found by the GMM model well.

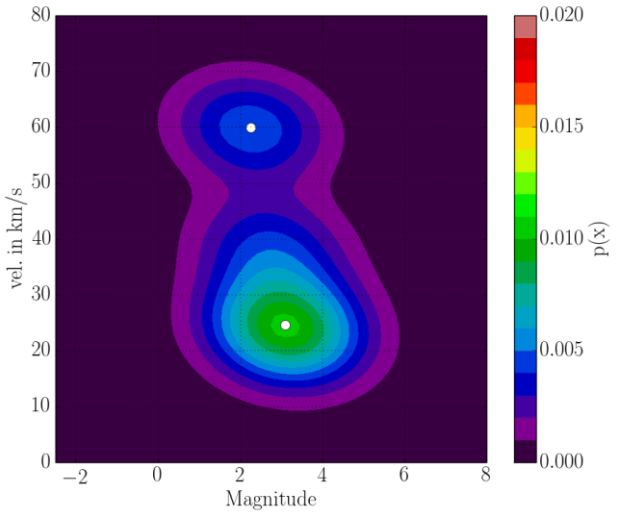

Figure 2 – PDF of the ICC7 velocity – magnitude data. The data range from 0 km/s to 80 km/s and from -2.5 mag to +8 mag. The PDF is described by four 2-dimensional Gaussians.

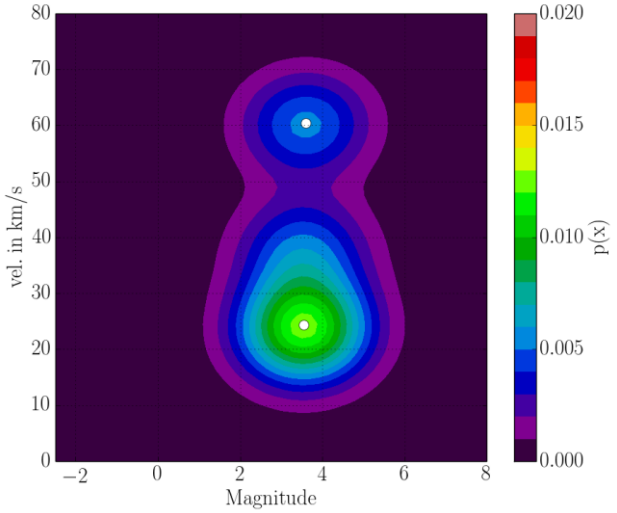

Figure 3 – PDF of the ICC9 velocity – magnitude data. The data range from 0 km/s to 80 km/s and from -2.5 mag to +8 mag. The PDF is described by four 2-dimensional Gaussians.

Table 2 lists the center values of both major clusters for both camera data sets. Both centers lay in the same velocity range. ICC7 and ICC9 detect mostly slow meteors with a mean velocity of approximately 24.5 km/s or rather fast meteors with a velocity of around 60 km/s, which is associated with sporadic meteors. However the cluster centers of ICC9 are shifted towards lower brightness measurements. The mean magnitude for the slow and fast meteors is shifted by 0.45 mag and around 1.35 mag, respectively. Both cameras are identical and are operated automatically in a similar manner. Thus the magnitude shift between both clusters cannot be explained by instrumental bias or dysfunctions.

Table 2 – Center coordinates of the two major data clusters of the ICC7 and ICC9 velocity – magnitude data

Camera	ICC7		ICC9	
Cluster Center	#1	#2	#1	#2
Bright. in mag.	3.10	2.25	3.55	3.60
Vel. In km/s	24.63	59.86	24.31	60.45

To explain the magnitude shift between ICC7 and ICC9 we analyze the angular velocity of each meteor across the CCD. *Figure 4* shows the normalized cumulative number of data points vs. the velocity in artificial CCD units (U) per second. 1 U is the height of the CCD sensor. The CCD sensor has a resolution of 576 x 768 pixels. Thus, the values along the CCD's width are normalized by a factor of 576/768 = 0.75. The solid curve represents the ICC7 data and the dashed line shows the ICC9 data. Both curves have been generated using a kernel density estimator. Each data point is replaced by a function kernel and the superposition of all functions generates the resulting distribution. Both distributions show the same progression until approximately 0.2 U/s. Approximately 50% of all velocities are within this interval. Afterwards the curves diverge significantly. The slope of the ICC9 curve is steeper and converges with the ICC7 distribution at around 1.0 U/s. For ICC9 90% of all velocities are smaller than 0.48 U/s, for ICC7 90% of all data are smaller than 0.64 U/s. Statistically, the simultaneously detected meteor data appear slower on the ICC9 CCD chip than on ICC7.

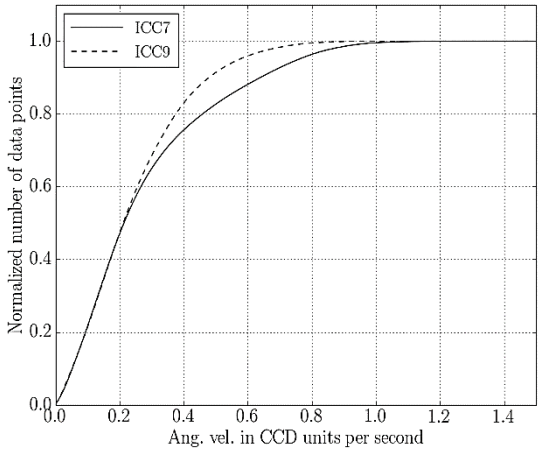

Figure 4 – Normalized cumulative distribution of the ICC7 and ICC9 angular velocity data. The velocity is given in relative CCD units (U) per second. 1 U is the height of the CCD and ranges from 0 to 1. The CCD has a resolution of 768 x 576 pixels. Thus the width values are normalized by a factor of 0.75.

Figure 5 shows the distribution of the mean angular velocity in U/s vs. the observation time of the meteor. The observation time is determined by n video frames

times 40 ms (both cameras capture 25 frames per second). Here all measurements are used from n = 3 to n = 20. The 1 sigma error varies between 0.1 and 0.2 U/s for both data sets. For a clear data representation the error bars are not shown, although they are considered. The dashed and solid line represent a Gaussian Process regression fit through the ICC7 and ICC9 data respectively, describing the function of the mean values. The gray-hatched areas show the 95% confidence interval for the mean values. Meteors with a length less than 120 ms (n=3) cannot be recorded and due to too few data and consequently large error bars meteor data with n > 20 have not been considered, too. Both fits are extended from 1 ms to 1,000 ms and the confidence interval broadening results from the mentioned data lack.

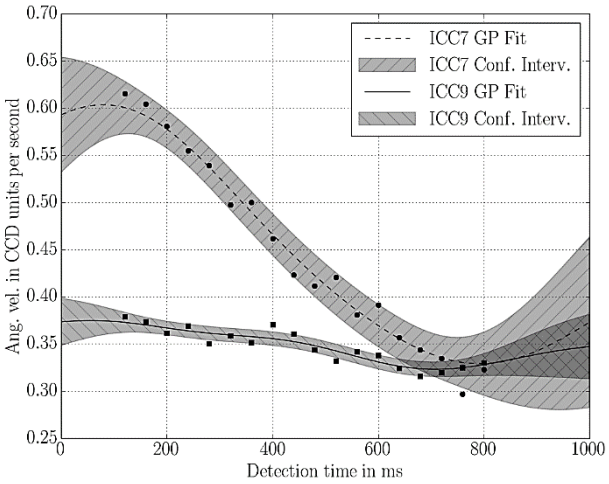

Figure 5 – Distribution of the meteor mean angular velocity in U/s vs. the meteor observation time. The data are obtained from 3 to 20 video frames long observations. The error bars are approximately 0.1 U/s large and are not shown for a clearer data representation. The dashed and solid line show a Gaussian Process (GP) fit. The hatched areas are the corresponding confidence intervals.

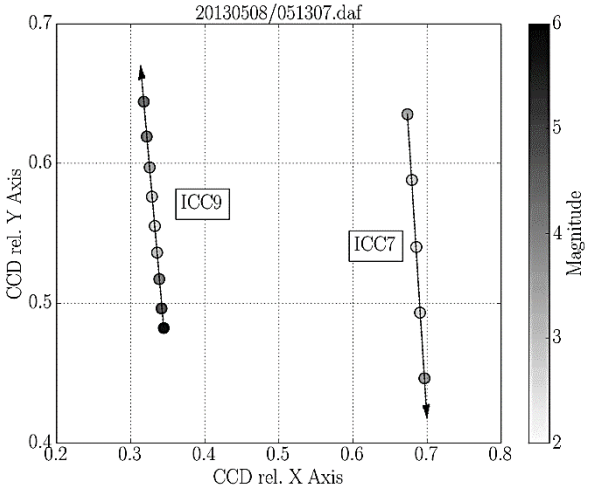

Figure 6 – Meteor position data from ICC7 and ICC9, merged in one CCD plot. The arrow indicates the flight direction, the dots represent the determined photometric center from each video frame. The gray scale shows the measured brightness in magnitudes.

It can be seen that the mean angular velocity for meteors captured with ICC7 decreases with the number of video frames. However, for ICC9 the data remain approximately constant around 0.35 U/s. Both mean fits converge for higher detection times and cross at around 800 ms. Meteors that only for a few 100 ms appear up to 80% faster on ICC7 than on ICC9.

This can be explained by the sporadic meteors coming from the Apex direction. During the night an observer on Earth revolves into the flight path of Earth. Meteors from this direction come from a rather diffuse radiant. The Apex radiant appears in the morning hours close to the horizon in the East and increases its altitude during the last hours of the night. Consequently, the number of observable Apex meteors increases during the last hours of the night.

ICC9's boresight is aimed eastwards while ICC7 is pointing roughly to the West. Thus, the angular distance is smaller between ICC9's boresight and the Apex, compared to ICC7. Meteors from the Apex therefore have a smaller angular velocity as seen from ICC9 than from ICC7. This explains *Figure 4*, which showed that ICC9 contains more data of meteors with a smaller angular velocity than ICC7. The smaller angular velocity means that the pixel dwell time of Apex meteors is smaller on the ICC9 camera chip than on ICC7. A smaller pixel dwell time causes a longer pixel illumination and a higher SNR. Both cameras use MetRec (Molau, 1999) as a detection software with the same detection threshold parameters. A higher SNR results in a better detectability, thus Apex meteors can be better detected with the ICC9 camera.

In general, the light curve of a meteor increases during the atmosphere entrance, reaches a maximum brightness and dims afterwards. An example of the trail of a simultaneously detected meteor is given in *Figure 6*. Each dot represents the meteor's photometric center on an ICC9 and ICC7 video frame. The angular velocity of the meteor is smaller on ICC9 than on ICC7. Furthermore ICC9 detected darker brightness values.

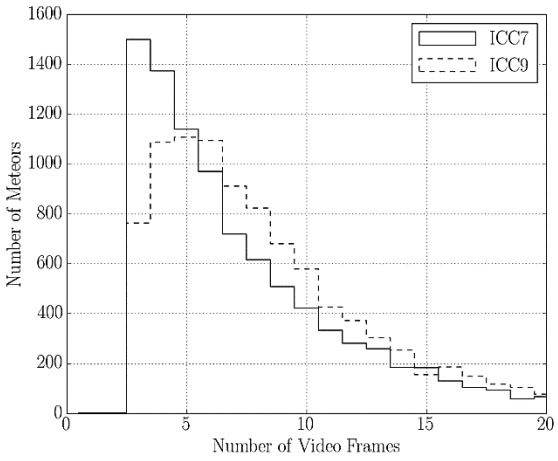

Figure 7 – Number of meteors vs. the number of video frames. Here only meteors are considered which appear fully on the CCD.

ICC9 detects more frames around the brightness maximum of an Apex meteor. This explains the distribution shown in *Figure 7*. ICC9 detects most

meteors on 5 frames while ICC7's distribution peak is at 3 frames. ICC9 detects fainter brightness values of an Apex meteor due to the better SNR. These additional fainter brightness measurements cause the cluster center shift shown in *Figure 3*. Although both cameras have the same set-up ICC9 is biased towards darker and slower meteor data.

Stream meteors could also contribute to the shown distributions. However Drolshagen and Ott (2014) have shown that the velocity distribution is dominated by the sporadic meteors.

4 CILBO's camera sensitivity

This Section describes the 2-dimensional CCD signal distribution of ICC7 and ICC9. In observational astronomy this analysis of an optical system is mostly done with a flat-field calibration. However, no proper flat field analysis, such as with a homogeneous extended light source, has been done for the CILBO system. *Figure 8 and 9* show a 2-dimensional detection distribution of all meteor position determinations. Here, all x-y CCD position values from the inf-files within the magnitude range +1 to +6 mag have been used. The density plot ranges in x and y direction from 0 to 1 and represents the complete CCD chip in normalized coordinates. The density is given in data points per u^2 and represents the artificial CCD coordinates. 1 u^2 stands here for the whole CCD chip. The density plot is computed with a kernel density estimator and the optimal bandwidth is determined with a cross validation algorithm.

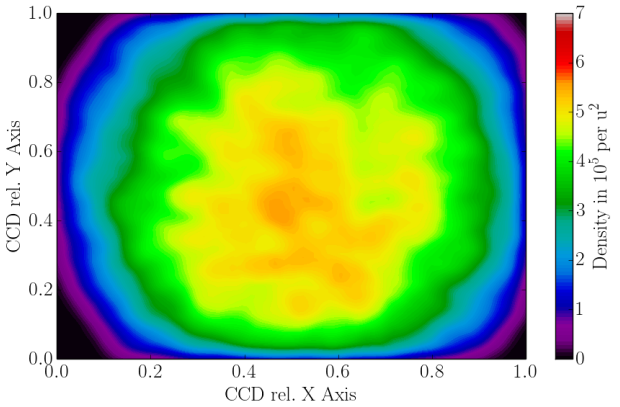

Figure 8 – Density plot showing the distribution of all determined photometric centers in CCD coordinates within the brightness range +1 mag to +6 mag (ICC7).

Both plots show a distribution with decreasing values to the edges and corners of the CCD. The values of each CCD decrease from the center to the edges along the x and y axis by a factor of up to 7. Additionally ICC9 shows a slight maximum offset towards smaller x and y coordinates. Both Figures result from optical distortion and the natural illumination falloff due to projection effects.

Assuming that all meteors come from any random direction at any time a uniform distribution would be expected. To estimate a possible detection loss the expected number of data points needs to be computed. This theoretical detection value is computed by extrapolating the maximum detection density along the whole CCD chip. This analysis focuses only on those meteors which are within the detection range of the CILBO system. The ratio between the theoretical expectation and the integral of the actual measurements is defined as the signal ratio *sr*. The signal ratios derived from *Figure 8 and 9* for ICC7 and ICC9 respectively are:

$$sr_{ICC7} = 0.609 \pm 0.002$$

$$sr_{ICC9} = 0.565 \pm 0.002$$

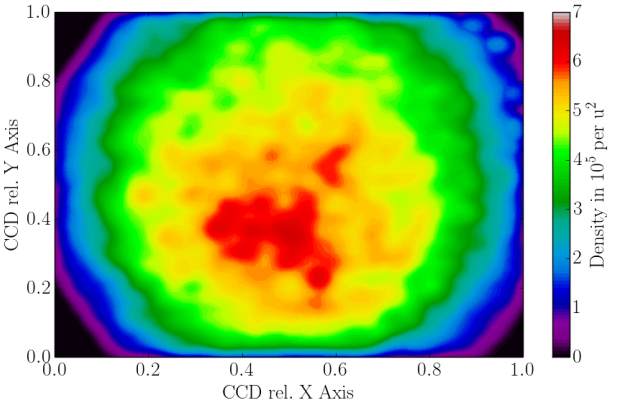

Figure 9 – Density plot showing the distribution of all determined photometric centers in CCD coordinates within the brightness range +1 mag to +6 mag (ICC9).

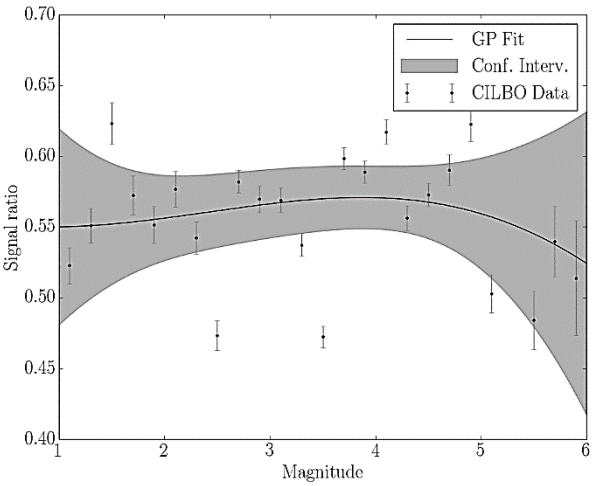

Figure 10 – Signal ratio vs. magnitude of ICC7 data. Each dot represents the signal ratio for a 0.2 mag interval. The fit and gray area show the GP fit and its confidence interval.

Both cameras have a signal loss of approximately 40% in the magnitude range +1 to +6 mag. Theoretically, the signal ratio should increase for brighter meteors. Thus, the data set is analyzed from +1 to +6 mag in 0.2 mag bins. For each magnitude bin, kernel density estimators are applied and the signal ratio is computed. The signal ratio results for both cameras can be seen in *Figure 10 and 11*. The data points for ICC7 are more scattered than ICC9. With a robust Gaussian Process algorithm a fit function has been determined for both data. The gray shaded area represents the confidence interval. Both fits predict a constant function along the magnitude range +2 to approximately +4.5 mag. Both confidence intervals diverge due to the lack of data points for brighter and

fainter meteors. However, considering the mean fit for ICC9 (solid line) the signal ratio increases for brighter and decreases for fainter meteors, respectively. Very bright meteors can be observed in the CCD center as well as close to the edges. Fainter meteors are only detectable close to the CCD's center. Thus the signal ratio decreases for higher magnitudes.

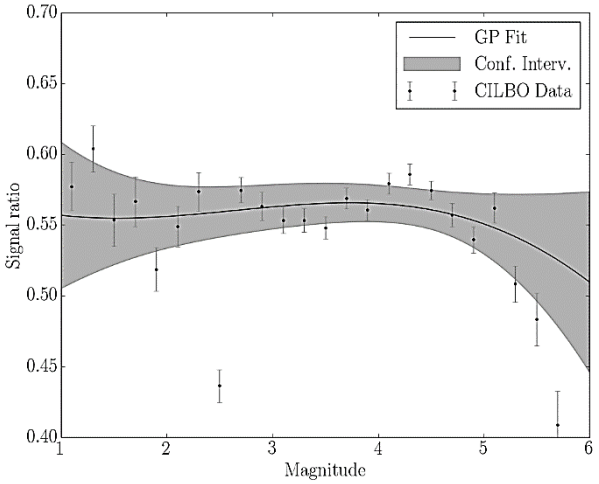

Figure 11 – Signal ratio vs. magnitude of ICC9 data. Each dot represents the signal ratio for a 0.2 mag interval. The fit and gray area show the GP fit and its confidence interval.

5 Summary / Outlook

In this paper we present a technical analysis of the Canary Islands Long-Baseline Observatory (CILBO) on Tenerife and La Palma. Our first analysis focuses on the pointing depending detection bias. Despite both cameras having a similar set-up, ICC9 detects more meteors that have a slower angular velocity on the CCD. This bias is caused by the sporadic Apex meteors. The diffuse radiant ascends during the morning hours in the East. Meteors from this region appear slower on the ICC9 camera due to its eastwards boresight pointing. Meteors with a slower angular velocity have a longer pixel dwell time. The effective exposure time per pixel is consequently higher and causes a better SNR. Faint meteors illuminate less pixels on ICC9 and trigger the detection software threshold faster. Simultaneously detected Apex meteors are consequently recorded on more ICC9 frames. The additional ICC9 video frames contain brightness data of the meteors at fainter states. These data cause the magnitude shift between both CILBO cameras and bias the data in regards of brightness, detection time and consequently trail length.

In a future analysis we will consider the time component and determine quantitatively the correlation between the found bias and the time-dependent angular distance between ICC7/ICC9 boresight and the Apex direction. Furthermore we will apply a proper meteor sorting. Here we used the whole CILBO meteor data set including sporadic meteors and stream meteors. To emphasize the Apex contribution our future analysis will only consider the sporadic background. However Drolshagen and Ott (2014) have already shown that the velocity distribution is significantly dominated by the sporadic meteors.

The second analysis investigates the CCD sensitivity of both cameras. Currently, no proper flat field measurement has been done for both instruments. Thus we used the observed meteors to determine a signal ratio of both cameras depending on the measured magnitude. We found for both cameras a signal ratio in the magnitude range +1 to +6 mag between 55% and 60%. We found, that the signal ratio of ICC9 increases and decreases for brighter and fainter meteors, respectively.

As the CILBO database grows, the results of this study will be improved, especially for ICC7. Further calibration methods, especially for a flat-field correction are currently theoretically investigated.

References

Drolshagen S., Kretschmer J., Koschny D., Drolshagen G., Poppe B. (2015). "Mass accumulation of Earth from interplanetary dust, meteroids, asteroids and comets". In Rault J.-L. and Roggemans P., editors, *Proceedings of the International Meteor Conference*, Mistelbach, Austria, 27-30 August 2015. IMO, pages 219–224.

Drolshagen E.,Ott T. (2014). "Meteoroid flux and velocity determination using image intensified video camera data from the CILBO double station". Bachelor thesis, unpublished.

Drolshagen E., Ott T., Koschny D., Drolshagen G., Poppe B. (2014). "Meteor velocity distribution from CILBO double station video camera data". In Rault J.-L. and Roggemans P., editors, *Proceedings of the International Meteor Conference*, Giron, France, 18-21 September 2014. IMO, pages 16–22.

Gruen E., Zook H. A., Fechtig H., Giese R. H. (1985). "Collisional balance of the meteoritic complex". *Icarus*, **62**, 244–273.

Kretschmer J., Drolshagen S., Koschny D., Drolshagen G., Poppe B. (2015). "De-biasing CILBO meteor observational data to mass fluxes". In Rault J.-L. and Roggemans P., editors, *Proceedings of the International Meteor Conference*, Mistelbach, Austria, 27-30 August 2015. IMO, pages 209–213.

Koschny D., and Diaz del Rio J. (2002). "Meteor Orbit and Trajectory Software (MOTS) - Determining the Position of a Meteor with Respect to the Earth Using Data Collected with the Software MetRec". *WGN, the Journal of the IMO*, **30**, 87–101.

Koschny D., Bettonvil F., Licandro J., v. d. Luijt C., Mc Auliffe J., Smit H., Svedhem H., de Wit F., Witasse O., Zender J. (2013). "A double-station meteor camera setup in the Canary Islands – CILBO". *Geosci. Instrum. Method. Data Syst.*, **2**, 339–348.

Koschny D., Mc Auliffe J., Bettonvil F., Drolshagen E., Licandro J., van der Luijt C., Ott T., Smit H., Svedhem H., Witasse O., and Zender, J. (2014). "CILBO - Lessons learnt from a double-station meteor camera setup in the Canary Islands". In Rault J.-L., and Roggemans P., editors, *Proceedings of the International Meteor Conference*, Giron, France, 18-21 September 2014. IMO, pages 10–15.

Koschny D., Albin T., Drolshagen E., Drolshagen G., Drolshagen S., Koschny J., Kretschmar J., van der Luijt C., Molijn C., Ott T., Poppe B., Smit H., Svedhem H., Toni A., de Wit F., Zender J. (2015). "Current activities at the ESA/ESTEC Meteor Research Group". In Rault J.-L. and Roggemans P., editors, *Proceedings of the International Meteor Conference*, Mistelbach, Austria, 27-30 August 2015. IMO, pages 204–208.

Molau S. (1999). "The Meteor Detection Software MetRec". In Arlt R. and Knoefel A., editors, *Proceedings of the International Meteor Conference*, Stara Lesna, Slovakia, 20 - 23 August 1998. IMO, pages 9–16.

Ott T., Drolshagen E., Koschny D., Drolshagen G., Poppe B. (2014). "Meteoroid flux determination using image intensified video camera data from the CILBO double station". In Rault J.-L., and Roggemans P., editors, *Proceedings of the International Meteor Conference*, Giron, France, 18-21 September 2014. IMO, pages 23–29.

Pedregosa F., Varoquaux G., Gramfort A., Michel V., Thirion B., Grisel O., Blondel M., Prettenhofer P., Weiss R., Dubourg V., Vanderplas J., Passos A., Cournapeau D., Brucher M., Perrot M., Duchesnay E. (2011). "Scikit-learn: Machine Learning in Python". *Journal of Machine Learning Research*, **12**, 2825–2830.

Vanderplas J. T., Connolly A. J., Ivezic Z., Gray A. (2012). "Introduction to astroML: Machine learning for astrophysics". *Conference on Intelligent Data Understanding (CIDU)*. October 2012, pages 47–54.

Vanderplas J. T., Connolly A. J., Ivezic Z., Gray A. (2014). "Statistics, Data Mining and Machine Learning in Astronomy". In Princeton University Press. Princeton, NJ.

The IMC participants in front of the Museum of Natural History, Vienna, Austria (Photo by *Christoph Niederhametner*).